Subunit-specific desensitization of heteromeric kainate receptors

David D. Mott[1], Asheebo Rojas[2], Janet L. Fisher[1], Raymond J. Dingledine[2] and Morris Benveniste[3]

[1]*Department of Pharmacology, Physiology and Neuroscience, University of South Carolina, School of Medicine, Columbia, SC 29208, USA*
[2]*Department of Pharmacology, Emory University School of Medicine, Atlanta, GA 30322, USA*
[3]*Neuroscience Institute, Morehouse School of Medicine, Atlanta, GA 30310, USA*

Kainate receptor subunits can form functional channels as homomers of GluK1, GluK2 or GluK3, or as heteromeric combinations with each other or incorporating GluK4 or GluK5 subunits. However, GluK4 and GluK5 cannot form functional channels by themselves. Incorporation of GluK4 or GluK5 into a heteromeric complex increases glutamate apparent affinity and also enables receptor activation by the agonist AMPA. Utilizing two-electrode voltage clamp of *Xenopus* oocytes injected with cRNA encoding kainate receptor subunits, we have observed that heteromeric channels composed of GluK2/GluK4 and GluK2/GluK5 have steady state concentration–response curves that were bell-shaped in response to either glutamate or AMPA. By contrast, homomeric GluK2 channels exhibited a monophasic steady state concentration–response curve that simply plateaued at high glutamate concentrations. By fitting several specific Markov models to GluK2/GluK4 heteromeric and GluK2 homomeric concentration–response data, we have determined that: (a) two strikingly different agonist binding affinities exist; (b) the high-affinity binding site leads to channel opening; and (c) the low-affinity agonist binding site leads to strong desensitization after agonist binding. Model parameters also approximate the onset and recovery kinetics of desensitization observed for macroscopic currents measured from HEK-293 cells expressing GluK2 and GluK4 subunits. The GluK2(E738D) mutation lowers the steady state apparent affinity for glutamate by 9000-fold in comparison to GluK2 homomeric wildtype receptors. When this mutant subunit was expressed with GluK4, the rising phase of the glutamate steady state concentration–response curve overlapped with the wildtype curve, whereas the declining phase was right-shifted toward lower affinity. Taken together, these data are consistent with a scheme whereby high-affinity agonist binding to a non-desensitizing GluK4 subunit opens the heteromeric channel, whereas low-affinity agonist binding to GluK2 desensitizes the whole channel complex.

(Received 25 November 2009; accepted after revision 18 December 2009; first published online 21 December 2009)
Corresponding author M. Benveniste: Neuroscience Institute, Morehouse School of Medicine, 720 Westview Drive, SW, Atlanta, GA 30310, USA. Email: mbenveniste@msm.edu

Abbreviations GluK (1–5), kainate receptor (1–5); Con A, concanavalin A; ATPA, 2-amino-3-(5-tert-butyl-3-oxo-1,2-oxazol-4-yl)propanoic acid.

Introduction

The glutamate-gated ion channel family is composed of three genetically and pharmacologically distinct subclasses: AMPA, kainate and NMDA receptors (Dingledine *et al.* 1999 for review). Kainate receptors function both presynaptically (Contractor *et al.* 2000; Schmitz *et al.* 2000; Frerking *et al.* 2001; Contractor *et al.* 2003; Fernandes *et al.* 2009) and postsynaptically (Castillo *et al.* 1997; Cossart *et al.* 2002; but see Kwon & Castillo, 2008), as studied intensely at the mossy fibre–CA3 synapse in the hippocampus as well as in hippocampal interneurons (Cossart *et al.* 1998; Frerking *et al.* 1998; Mulle *et al.* 2000; Rodriguez-Moreno *et al.* 2000; Pinheiro *et al.* 2007; Mott *et al.* 2008), thalamocortical synapses in the barrel cortex (Kidd *et al.* 2002; Bannister *et al.* 2005) and dorsal root ganglion neurons (Wilding & Huettner, 1996). Although many physiological functions of kainate receptors have not been clearly elucidated, these receptors may be involved in generation of seizures in some models of epilepsy (Mulle *et al.* 1998; Smolders *et al.* 2002).

A general issue for understanding the functions of any multi-subunit protein is the extent to which each subunit contributes an independent modular function,

DOI: 10.1113/jphysiol.2009.185207

compared with a situation in which the combination of subunits induces an emergent property not predicted by the properties of individual subunits. The kainate receptor subclass contains five different subunits. GluK1, GluK2 and GluK3 (formerly GluR5–7) can be expressed as homomeric or heteromeric channels, whereas homomeric GluK4 or GluK5 channels (formerly KA1 and KA2) are non-functional and must be expressed in combination with GluK1/3 (Ren *et al.* 2003; Nasu-Nishimura *et al.* 2006). Inclusion of GluK4 or GluK5 subunits in heteromeric assemblies with GluK1 or GluK2 confers different pharmacological properties on the resulting channel. For instance, AMPA, ATPA and iodowillardine, which do not induce significant currents through GluK2 homomeric channels, can activate the GluK2/GluK5 subunit combination (Swanson *et al.* 1998; Paternain *et al.* 2000; Alt *et al.* 2004). Dysiherbaine, a high-affinity kainate receptor agonist, elicits practically irreversible desensitization of GluK1 and GluK2 homomeric channels, but when GluK5 subunits are co-expressed with GluK2, recovery from desensitization occurs within minutes (Swanson *et al.* 2002). Expression of GluK5 subunits with the edited (R) forms of either GluK1 or GluK2 also significantly increases single channel conductances (Swanson *et al.* 1996).

Although GluK4 and GluK5 subunits are non-functional as homomeric channels, when expressed as homomers in HEK-293 cells they bind kainate and glutamate with higher affinity than their GluK1/3 counterparts (Werner *et al.* 1991; Herb *et al.* 1992). Upon removal of dysiherbaine from HEK-293 cells expressing GluK1/GluK5 heteromeric channels, long lasting tail currents were observed; however, tail currents were not observed for GluK1 homomeric channels (Swanson *et al.* 2002). These tail currents suggest that dysiherbaine is dissociating from its binding sites at two vastly different rates, implying that functional high- and low-affinity agonist binding sites may exist on heteromeric channels.

In this study, we show that heteromeric kainate receptors have bell-shaped, biphasic steady state concentration–response curves that result from differential activation of GluK4 or GluK5 subunits with high affinity for agonist and GluK2 subunits with low affinity for agonist. Binding of agonist to GluK2 subunits strongly desensitizes the channel complex, and is responsible for the falling phase of the biphasic agonist concentration–response curve, whereas GluK4 or K5 subunits are relatively non-desensitizing and primarily responsible for the rising (activation) phase of the concentration–response curve.

Methods

All procedures involving animals conformed to the guidelines of the Animal Care and Use Committee of Emory University. All chemicals were purchased from Sigma (St Louis, MO, USA) except S-AMPA, which was purchased from Tocris Bioscience (Ellisville, MO, USA).

Oocyte expression system and recordings

The GluK2(E738D) mutant (Mah *et al.* 2005) was generated from the GluK2(R) wildtype cDNA in a pGEM vector using the QuickChange site-directed mutagenesis kit (Stratagene, La Jolla, CA, USA). The GluK2(E738D) mutant vector was verified by DNA sequencing. The GluK2-containing plasmid was a generous gift from M. Mayer (National Institutes of Health, Bethesda, MD, USA). GluK4- and GluK5-expressing plasmids were generously provided by S. Heinemann (Salk Institute, San Diego, CA, USA). All cRNAs were transcribed *in vitro* from linearized cDNA templates utilizing the mMessage mMachine kit (Ambion, Austin, TX, USA).

Stage V–VI *Xenopus laevis* oocytes were removed from frogs that had been anaesthetized in water containing 0.156% tricaine. After treatment with type IV collagenase (1.7 mg ml^{-1} for 45–120 min; Worthington Biochemical, Lakewood, NJ, USA) in a calcium-free Barth's solution, oocytes were injected with either GluK2(R) cRNA (50 ng), or GluK2(R) (7.5 ng) together with GluK4 (50 ng) or GluK5 (50 ng) cRNA. Injected oocytes were maintained in Barth's solution containing (in mM): NaCl 88, $NaHCO_3$ 2.4, KCl 1, $Ca(NO_3)_2$ 0.33, $CaCl_2$ 0.41, $MgSO_4$ 0.82, Tris/HCl (pH = 7.4) 5, and supplemented with penicillin (10 U ml^{-1}) and streptomycin (10 μg ml^{-1}) at 17°C for 3–10 days before electrophysiological recording (Mott *et al.* 2003). Agonist-evoked steady state currents for expressed recombinant kainate receptors were acquired utilizing two-electrode voltage clamp facilitated by an Axoclamp 2A amplifier (Molecular Devices, Sunnyvale, CA, USA). Recording pipettes were filled with a solution containing 3 M CsCl and 0.4 M EGTA. During recordings, oocytes were continually perfused with standard frog Ringer solution containing (in mM): NaCl 90, KCl 1, HEPES 15, $MgCl_2$ 0.4, $CaCl_2$ 0.1 (pH = 7.4). GluK2 homomeric receptors were activated by bath application of glutamate. GluK2/GluK4 and GluK2/GluK5 receptors were activated by bath application of glutamate or AMPA. Currents were elicited from a holding potential of −60 mV unless otherwise specified. Signals were digitized at 100 Hz with a Digidata 1200 analog-to-digital converter (Molecular Devices) under the control of pCLAMP 9.2 acquisition software (Molecular Devices). After final collection of *Xenopus* oocytes, frogs were humanely killed by emersion in tricaine (0.156%) for 2 h.

Mammalian expression system and recordings

GluK2(Q) in the cytomegalovirus-based mammalian expression vector JG3.6 was a gift from S. Heinemann.

For these experiments, the GluK4 plasmid from the Heinemann laboratory was subcloned into the pCIneo vector (Promega Corporation, Madison, WI, USA) for use in mammalian cells. Mammalian expression of kainate receptors was done by transfecting human embryonic kidney cells (HEK-293T, GenHunter, Nashville, TN, USA) with cDNA plasmids by calcium phosphate precipitation. For expression of GluK2 homomers, 2 μg of cDNA were used. For expression of GluK2/GluK4 heteromeric channels, 1 μg of GluK2 was combined with 3 μg of GluK4. 1 μg of a cDNA encoding a single chain antibody recognizing the hapten 4-ethoxymethylene-2-phenyl-2-oxazolin-5-one (phOx) was also transfected into the cells as a marker for transfection (Chesnut *et al.* 1996). Cells were incubated with the DNA solution for 4–6 h at 3% CO_2 followed by treatment with a 15% glycerol solution in BES buffer (50 mM *N*,*N*-*bis*[2-hydroxyethyl]-2-aminoethanesulfonic acid, 280 mM NaCl, 1.5 mM Na_2HPO_4) for 30 s. Cells underwent a selection procedure 20–28 h after transfection in which they were passaged and then incubated with 3–5 μl of magnetic beads (approximately 5×10^5 beads) conjugated with the phOx–BSA (Chesnut *et al.* 1996) for 30–60 min. Positively transfected cells were then isolated with a magnetic stand and plated onto glass coverslips treated with poly-L-lysine and collagen, maintained in Dulbecco's modified Eagle medium containing 10% fetal bovine serum, 100 IU ml^{-1} penicillin and 100 μg ml^{-1} streptomycin, and used in electrophysiological experiments 20–28 h later.

Measurements of the onset and recovery of desensitization were made under voltage clamp utilizing an Axopatch 200B amplifier (Molecular Devices) from excised outside-out patches pulled from the positively transfected cells. The intracellular solution contained (in mM): caesium gluconate 130, CsCl 5, HEPES 10, Cs_4BAPTA 5, $MgCl_2$ 2, MgATP 2 and NaGTP 0.3, and was titrated to pH 7.3 and 290 mosmol l^{-1}. The extracellular solution contained (in mM): NaCl 150, KCl 3, HEPES 10, $CaCl_2$ 1 and $MgCl_2$ 0.4, and was titrated to pH 7.4 and 300 mosmol l^{-1}. Glutamate was rapidly applied to patches using a stepper solution exchanger (SF-77B, Warner Instruments, Hamden, CT, USA). The 3-barrel square glass was pulled to a final total width for the three barrels between 200–400 μm. The 10–90% rise times of the junction potential at the open tip were consistently faster than 400 μs as tested using a diluted external solution. Signals were digitized at 10 kHz under the control of pCLAMP 9.2.

Analysis

Biphasic concentration–response curves were fitted with a general logistic equation that describes a bell-shaped concentration–response curve (Nahum-Levy *et al.* 1999):

$$100 \times \frac{I}{I_N} = \frac{\left(\left(\frac{[\text{Agonist}]}{A_{1/2}}\right)^{n_e}\right) A_{max}}{\left(1+\left(\frac{[\text{Agonist}]}{A_{1/2}}\right)^{n_e}\right)\left(1+\left(\frac{[\text{Agonist}]}{I_{1/2}}\right)^{n_i}\right)} \quad (1)$$

where I is the steady state current, I_N is the steady state current at the normalizing concentration, A_{max} is the projected maximal response, $A_{1/2}$ is the concentration for the half-maximal agonistic effect, and $I_{1/2}$ is the half-maximal concentration for the antagonist effect. n_e and n_i are the Hill coefficients corresponding to the agonistic and antagonistic effects, respectively. Monophasic concentration–response curves were fitted with a standard logistic equation of the form:

$$100 \times \frac{I}{I_{max}} = \frac{A_{max}}{1+\left(\frac{A_{1/2}}{[\text{Agonist}]}\right)^{n_e}} \quad (2)$$

where I_{max} is the maximal steady state current evoked by agonist. All data analysis and fits were done with Igor Pro 6 (Wavemetrics Inc., Lake Oswego, OR, USA).

Simulations and fitting of currents under voltage clamp to specific receptor models were performed using code originally written by John Clements (Benveniste *et al.* 1990), revised and converted by M.B. to an Igor Pro XOP. Receptor state occupancies at each time point were determined numerically by calculating the change in each state occupancy resulting from transitions into and out of each state according to first order reaction rate kinetics as detailed in Benveniste *et al.* (1990). This was done iteratively at least 20 times per time point. Steady state agonist concentration–response curves were normalized to the response produced by a standard concentration and fitted by minimizing the χ^2 error between normalized steady state values and normalized simulated responses using internal IGOR algorithms, which are based on the Levenberg–Marquardt non-linear least-squares algorithm. For the fits, data points were weighted with their respective standard deviations. For analysis of steady state concentration–response data, reaction rates have no meaning. For this reason, ligand association rates were kept constant and dissociation rate constants allowed to vary in order to determine equilibrium dissociation constants for each transition. Since a variety of kinetic constants could be used to simulate the steady state data, we also verified if the constants used produced simulations in which the kinetics of onset and recovery from desensitization were similar to data acquired from HEK-293 cells (Fig. 3).

The main model used in this study (Fig. 4*C*) is based on the activation and desensitization models for homomeric AMPA receptors of Robert and Howe, in which the binding of two agonist molecules is required for channel opening and multiple levels of desensitization are possible (Robert & Howe, 2003; Robert *et al.* 2005). However, instead of having macroscopic transitions between four equivalent homomeric subunits, our heteromeric receptor model assumes that there are two GluK2 subunits and two GluK4 (or K5) subunits. To simplify the models, transitions for channel opening (β) and closing (α) were universally set to 500 and 10 000 s^{-1}, respectively, and all open states had the same conductance. These simplifications are justified because changing the transition rates to and from the open state and changing conductances of the various open states were tested extensively and did not influence whether agonist steady state concentration–response curves would be monophasic or biphasic, nor did they greatly change the fold difference in affinities observed between agonist binding states. A full listing of the transitions for each model is presented in the online Supplementary Material. Simulations and fitting were run on a Macintosh MacBook Pro computer. Error bars on graphs are standard deviations of the mean.

Results

Heteromeric kainate receptors yield biphasic agonist concentration–response curves

Oocytes injected with GluK2 cRNA transcripts elicited inward currents at a holding potential of −60 mV when they were exposed to different concentrations of glutamate (Fig. 1*A*). Increasing the concentration of glutamate

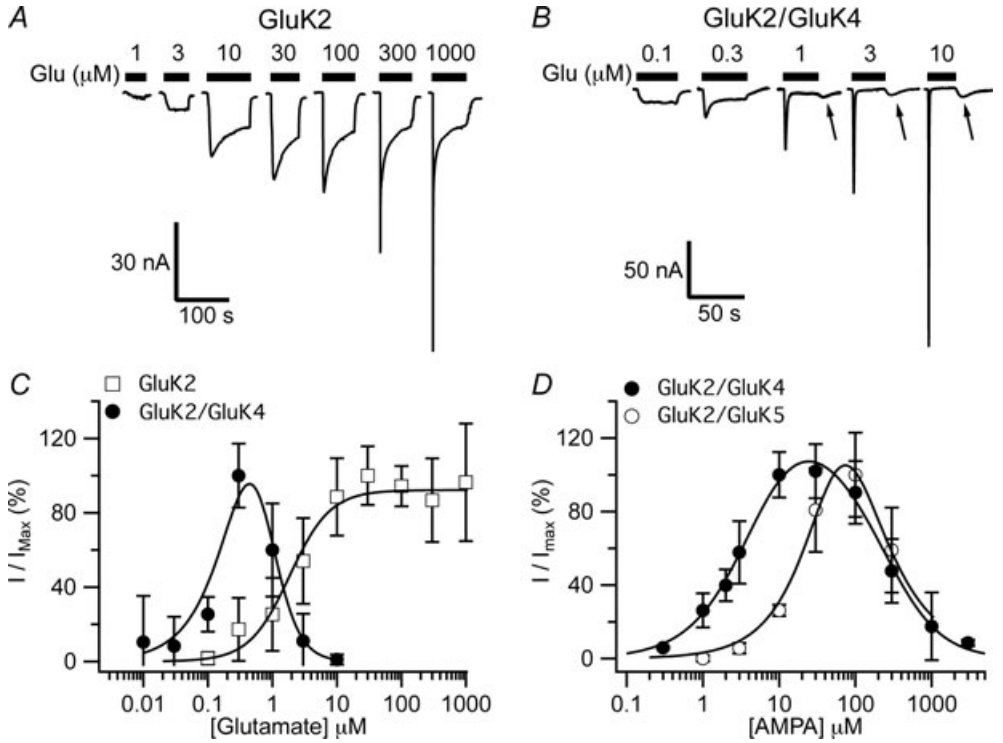

Figure 1. Heteromeric GluK2/GluK4 and GluK2/GluK5 channels have biphasic steady state responses to glutamate

A, an example of raw data traces during application of glutamate (Glu) to an oocyte expressing homomeric GluK2 channels under voltage clamp. Both peak and steady state responses increase with increasing glutamate concentrations. *B*, voltage clamp current traces from an oocyte expressing GluK2/GluK4 channels. Although peak responses increase with increasing glutamate, steady state currents decrease above 0.3 μM. Arrows indicate the emergence of a 'tail' current that appears after removal of glutamate. *C*, steady state glutamate concentration–response curves for homomeric GluK2 (open squares) and heteromeric GluK2/GluK4 (filled circles) expressing oocytes. Currents (I) recorded under voltage clamp at different glutamate concentrations were normalized to their maximal steady state responses at 0.3 μM and 30 μM glutamate (I_{max}) for GluK2/GluK4 and homomeric GluK2-expressing oocytes, respectively. Smooth lines indicate fits to eqns (1) and (2) for GluK2/GluK4 and GluK2, respectively. Fit parameters: GluK2/GluK4: $A_{1/2} = 89$ nM, $n_e = 1.6$, $I_{1/2} = 764$ nM, $n_i = 1.6$, $A_{max} = 315\%$; GluK2: $A_{1/2} = 1.8$ μM; $n_e = 1.3$. *D*, AMPA also yields a biphasic steady state concentration–response curve from oocytes expressing GluK2/GluK4 (filled circles) and GluK2/GluK5 (open circles). Smooth lines represent fits to eqn (1). Fit parameters: GluK2/GluK4: $A_{1/2} = 5.8$ μM, $n_e = 1.1$, $I_{1/2} = 329$ μM, $n_i = 1.2$, $A_{max} = 163\%$; GluK2/GluK5: $A_{1/2} = 68$ μM, $n_e = 1.4$, $I_{1/2} = 298$ μM, $n_i = 1.4$, $A_{max} = 239\%$.

produced a monotonic increase in both peak and steady state responses. Steady state responses could be fitted with eqn (2), yielding an $A_{1/2}$ value of 1.8 μM and a Hill coefficient (n_e) of 1.3 (open squares in Fig. 1*C*, $n = 12$ oocytes). In contrast, when GluK2 and GluK4 subunit transcripts were co-expressed in oocytes and examined under voltage clamp, steady state currents reached a maximal inward response at approximately 0.3 μM glutamate but decreased back to baseline with increasing concentrations of glutamate (Fig. 1*B*). This biphasic concentration–response relationship could be fitted with eqn (1), which empirically attributes the rising and decaying phase of the data to two apparent affinities of the same agonist. Due to the large number of parameters in eqn (1), reliable fits could not be obtained without setting the Hill coefficients, n_e and n_i to a constant. Setting n_e and n_i to 1.6 resulted in the best fit. $A_{1/2}$ and $I_{1/2}$ values determined from the fit of currents from heteromeric GluK2/GluK4 channels were 689 and 764 nM, respectively ($n = 12$ oocytes). A_{max}, the potential maximum response resolved from this fit was 315%, a value more than 3-fold higher than the highest relative response (Fig. 1*C*).

The biphasic steady state concentration–response curves produced by GluK2/GluK4 channels could result from a specific interaction of glutamate with the heteromeric channel, or could occur with any kainate receptor agonist. In addition, steady state currents evoked by glutamate are very small (Fig. 1*A* and *B*) and small fluctuations in leak current or endogenous activation of other currents by glutamate could influence analysis. AMPA is also an agonist of heteromeric GluK2-containing channels, yields larger steady state currents, and has been reported to not elicit currents from GluK2 homomeric channels (Herb *et al.* 1992; Swanson *et al.* 1997). Figure 1*D* indicates that steady state activity of GluK2/GluK4 and GluK2/GluK5 heteromeric channels elicited by AMPA also have biphasic concentration–response relationships. Fits to these AMPA concentration–response curves for GluK2/GluK4 heteromeric channels yielded $A_{1/2}$ and $I_{1/2}$ values of 5.8 and 329 μM, respectively, with Hill coefficient n_e fitted to 1.1 ($n = 29$ oocytes). In order to obtain a successful fit, n_i had to be held constant at 1.2. AMPA concentration–response curves were also acquired for oocytes expressing GluK2/GluK5 channels (Fig. 1*D*, open circles). Analysis of the GluK2/GluK5 data yielded $A_{1/2}$ and $I_{1/2}$ values of 67 and 298 μM, respectively ($n = 5$ oocytes). To successfully fit these data, both n_e and n_i had to be held constant (1.4 and 1.2, respectively).

All GluK2/GluK4 and GluK2/GluK5 responses to high concentrations of either glutamate (>1 μM) or AMPA (>100 μM) produced a peak inward 'tail' current upon removal of the agonist (Figs 1*B* and 2*A*). Although solution exchange in our oocyte recording chamber is several seconds, this tail current cannot solely result from slow solution exchange since responses from GluK2 homomeric channels to high concentrations of glutamate did not yield tail currents upon agonist removal (Fig. 1*A*). The presence of such tail currents could be caused by rapid dissociation of agonist from a low-affinity 'inhibitory' binding site on the channel prior to complete dissociation from binding sites that cause channel opening. Together, the biphasic nature of the steady state concentration–response data combined with the observation of 'tail' currents upon removal of high concentrations of agonist suggest that glutamate and AMPA activate heteromeric GluK2/GluK4 and GluK2/GluK5 channels through a high apparent affinity site and inhibit the channel through a low apparent affinity binding site.

We postulated that the putative low apparent affinity inhibitory response may result from channel desensitization. To test this, we elicited responses to glutamate on GluK2/GluK4 channels in the presence and absence of the lectin concanavalin A (Con A), which

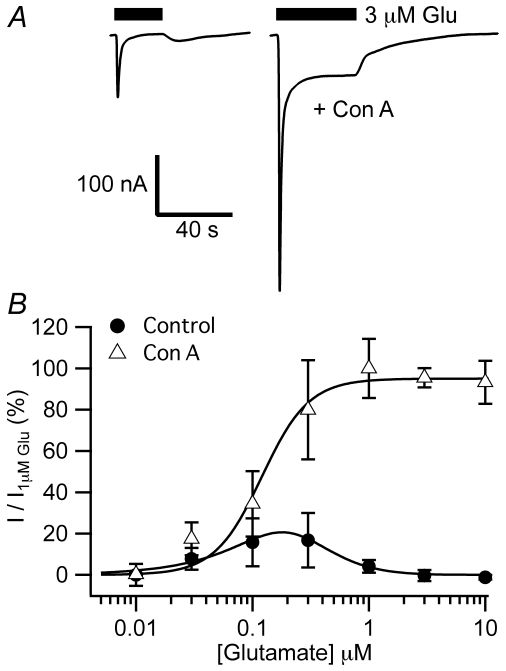

Figure 2. Partial block of desensitization of GluK2/GluK4 channels produces a monophasic steady state concentration–response curve to glutamate
A, an example of currents elicited by 3 μM glutamate on an oocyte expressing GluK2/GluK4 channels in the presence and absence of 0.3 mg ml^{-1} Con A. *B*, averaged data from 4 oocytes expressing GluK2/GluK4 for which glutamate concentration–response curves were collected in the presence (open triangles) and absence (filled circles) of Con A on each oocyte. Data are normalized to the steady state maximal response measured in the presence of Con A and 1 μM glutamate. Smooth lines indicate fits to eqns (1) and (2) for responses in the absence and presence of Con A, respectively. Fit parameters: Control: $A_{1/2} = 210$ nM, $n_e = 2.1$, $I_{1/2} = 1.0$ μM, $n_i = 1.4$, $A_{max} = 45.2\%$; +Con A: $A_{1/2} = 120$ nM; $n_e = 2.1$

can block desensitization of kainate receptors (Huettner, 1990; Wong & Mayer, 1993). Incubation with 0.3 mg ml^{-1} Con A caused steady state GluK2/GluK4 responses to increase significantly (Fig. 2*A*). 'Tail' currents elicited upon removal of agonist were no longer present and the glutamate concentration–response curve increased monotonically in the presence of Con A (Fig. 2*B*, open triangles). Fits (utilizing eqn (2)) to glutamate-induced steady state responses from GluK2/GluK4 channels in the presence of Con A yielded an $A_{1/2}$ value of 120 nM and a n_e of 2.1 ($n = 4$ oocytes). Note that responses to low concentrations of glutamate in the presence of Con A significantly overlap with the rising phase of the biphasic concentration–response curve acquired in the absence of Con A in the same oocytes (Fig. 2*B*). These results strengthen the notion that desensitization may be responsible for the declining phase of the glutamate and AMPA concentration–response curves from GluK2/GluK4 and GluK2/GluK5 channels.

Comparison of desensitization kinetics for GluK2- and GluK2/GluK4-containing channels

Before we determined which models of activation and desensitization may fit the acquired biphasic concentration–response curves (Fig. 1*C* and *D*), we wished to determine the kinetics for the onset and recovery of desensitization of GluK2/GluK4 channels. HEK-293T cells were transfected with GluK2 cDNA alone or in combination with GluK4 cDNA. To determine the rate of onset of desensitization, 10 μM or 1 mM glutamate were applied to excised patches expressing these channels for either 1 s or 100 ms, respectively (Fig. 3*A* and *B*). In the presence of 1 mM glutamate, responses from GluK2- and GluK2/GluK4-expressing outside-out patches yielded similar exponential decays of 5.4 ± 1.8 ms ($n = 9$ patches) and 4.4 ± 0.8 ms ($n = 8$ patches), respectively (Fig. 3*C*). The onset of desensitization was slower for applications of 10 μM glutamate. Time constants of decay were

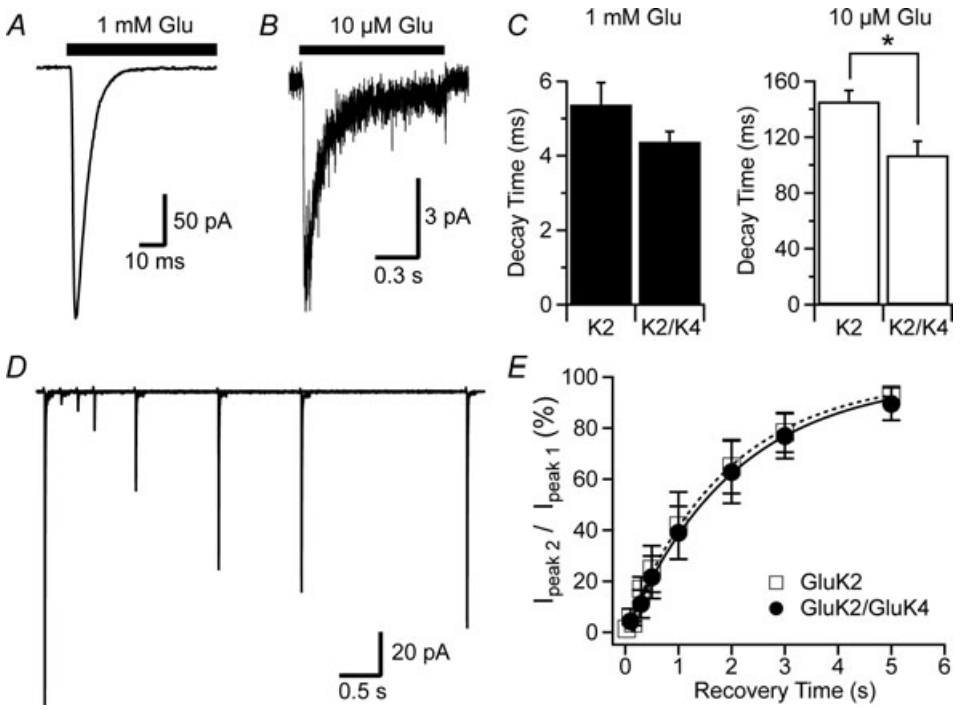

Figure 3. Desensitization kinetics of homomeric GluK2 and GluK2/GluK4 receptors
Patches from HEK-293 cells expressing GluK2 alone or in combination with GluK4 were held under voltage clamp and exposed to glutamate utilizing a rapid application system. *A*, current recorded from a patch expressing GluK2 and GluK4 subunits during a 1 mM glutamate application for 100 ms. *B*, current recorded from a different patch expressing GluK2 and GluK4 subunits during a 1 s application of 10 μM glutamate. *C*, summary of the onset of desensitization by the measurement of the time constant of current decay for the conditions described in *A* and *B* for both GluK2 homomeric receptor channels and GluK2/GluK4 channels. *D*, example traces which were acquired during a paired-pulse protocol where each pulse was 1 mM glutamate for 100 ms. The traces show the recovery from desensitization in a single patch expressing GluK2 and GluK4 subunits. *E*, analysis of the normalized paired-pulse data indicates similar rates of recovery from desensitization for homomeric GluK2- and GluK2/GluK4-containing patches.

145.5 ± 25.0 ms ($n = 10$ patches) and 107.1 ± 26.5 ms ($n = 7$ patches) for GluK2 and GluK2/GluK4, respectively. Recovery from desensitization was measured using a paired-pulse protocol in which 1 mM glutamate was pulsed twice for 100 ms at varying intervals (Fig. 3*D*). The peak response from the second glutamate pulse was normalized to that of the first and fitted to a single exponential function. Recovery time constants for GluK2 and GluK2/GluK4 were 1.94 ± 0.46 s ($n = 6$ patches) and 2.02 ± 0.52 s ($n = 6$ patches), respectively (Fig. 3*E*). The fact that recovery from desensitization is similar for channels composed solely of GluK2 subunits or GluK2 and GluK4 subunits may suggest that similar molecular determinants may be involved in this process. In addition, the dependence of the onset of desensitization on glutamate concentration will be useful in establishing constants for agonist binding and desensitization parameters within our models.

Modelling activation and desensitization of heteromeric GluK2/GluK4 subunits

Binding and desensitization schemes can be constructed to represent specific mechanistic steps in the activation and desensitization of kainate receptors. Simulated currents can then be produced from the occupancies of the conducting states of these schemes. Then, the validity of these mechanistic models can be determined by how well simulated currents represent our electrophysiological data. We tested several models of activation and desensitization to see which would best reproduce the biphasic steady state concentration–response curve. For simplicity, all models assume that activation can occur upon the binding of at least two molecules of agonist, and that transition to a desensitized state requires the binding of one molecule of agonist. Heterologously expressed homomeric GluK4 or K5 subunits bind kainate (Werner *et al.* 1991; Herb *et al.* 1992), but are non-functional (Ren *et al.* 2003; Nasu-Nishimura *et al.* 2006). Although dysiherbaine and its analogues functionally interact with the GluK5 subunit in heteromeric kainate receptors (Swanson *et al.* 2002; Sanders *et al.* 2005, 2006), it has not been explicitly shown that glutamate can bind and function as an agonist with GluK4 or GluK5 subunits in heteromeric combination with GluK2. For this reason, we first explored two activation schemes in which the GluK4 subunit does not bind glutamate but still confers an extra degree of desensitization in addition to that caused by GluK2 subunits (Fig. 4*A*). In the serial activation scheme, binding of glutamate must first cause desensitization of the GluK2 subunit prior to desensitization of the GluK4 subunit or the converse. In the parallel activation scheme, binding of agonist can lead to desensitization of either GluK2 or GluK4 subunits. Serial desensitization schemes produced simulated steady state responses that were monotonically increasing with increasing glutamate concentration (Fig. 4*B*) and thus did not yield a good fit. Parallel desensitization schemes had a similar trend (not shown). Fits of the steady state glutamate concentration–response curves to either model were poor with large χ^2 errors (Table 1).

Next, we tried an activation model for heteromeric channels in which both GluK2 and GluK4 subunits can bind agonist with different affinities; binding to either subunit promotes both channel opening and desensitization. The general model used for this and additional simulations in this study is presented in Fig. 4*C*. In Fig. 4*D*, the purple line serves as a reference to show that when using the model presented in Fig. 4*C* with the glutamate binding affinity at both sites set to the same affinity, a monotonically increasing glutamate concentration-response is observed. Simulations with this model where glutamate binding had strikingly different affinities at each subunit also produced steady state concentration–response curves that all had increasing responses with increasing glutamate concentration as long as each subunit had the same strongly desensitizing equilibrium (green line in Fig. 4*D*). Finally, we allowed both the glutamate binding affinities and the desensitization equilibria for the two types of subunits to vary in a fit of the biphasic concentration–response curve data. Due to the large number of variables relative to the number of data points, data could not be fitted with four variable parameters. With three variable parameters (K_d for GluK2 and GluK4 and K_{desens} for GluK2), we found that the glutamate low binding affinity always associated with a strongly desensitizing equilibrium ($K_{desens} \ll 1$) and the glutamate high binding affinity associated with the non-desensitizing equilibrium ($K_{desens} = 10$). However, upon further testing, the fitted parameters yielded a simulated recovery from desensitization which was too slow (data not shown) in comparison to experimental data (Fig. 3*E*). The recovery from desensitization was then manipulated to yield simulated data which matched experimental data, and then the concentration–response data was refitted with the model depicted in Fig. 4*C* with only the K_d for GluK2 and GluK4 being variable. Again, the resulting fit indicated that the strongly desensitizing subunit had a low affinity for glutamate and the non-desensitizing subunit had a higher affinity for glutamate. Results from this two free parameter fit are presented in Fig. 4*D* (blue continuous line) and Table 1, where we have arbitrarily chosen to label the GluK2 subunit as the strongly desensitizing subunit, because we know that it desensitizes strongly in GluK2 homomeric receptors (Kohler *et al.* 1993; Heckmann *et al.* 1996). Additional simulations confirmed that as long as the low-affinity glutamate binding subunit was strongly desensitizing, a biphasic fit was produced. When the strongly desensitizing subunit (GluK2) was forced to have

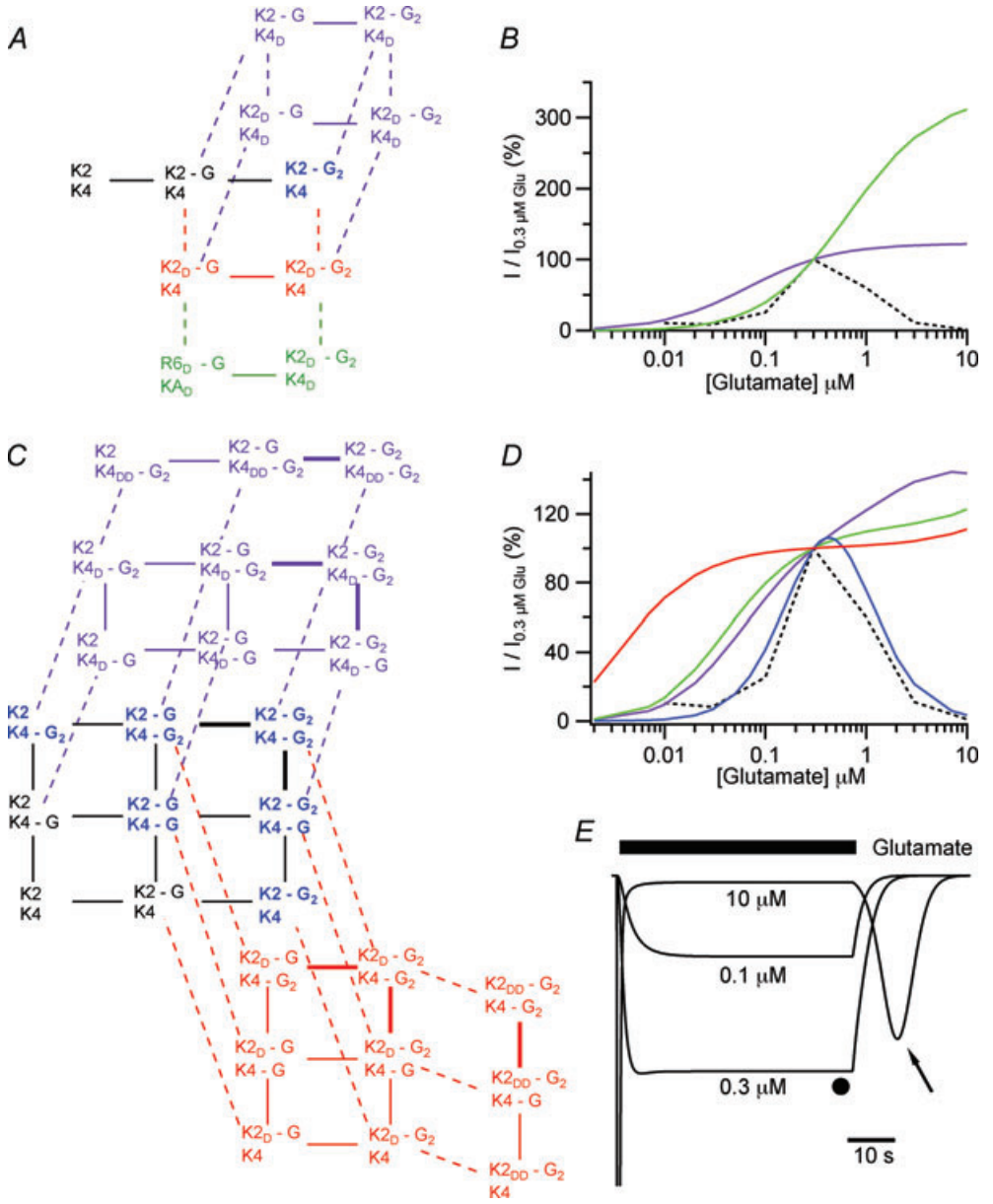

Figure 4. Acceptable fits of glutamate concentration–response curves require a model with both low-affinity, strongly desensitizing subunits and high-affinity, non-desensitizing subunits
All models depicted contain two GluK2 subunits (K2) and two GluK4 or GluK5 subunits (K4). Subscript 2 indicates that both subunits are bound with glutamate, whereas lack of a subscript indicates that only one of the subunits has glutamate bound. Subscript D indicates one desensitized subunit, DD indicates that both subunits of the subtype are in desensitized states. Binding transitions are depicted as continuous lines, desensitization transitions are depicted as dashed lines. Embolden blue states can directly transition to open states (which are not shown). *A*, two models in which the GluK4 subunit does not bind glutamate (G) but can confer an additional desensitization state on the channel. The serial desensitization model is composed of black, red and green transitions. The parallel desensitization model is composed of black, red and purple transitions. *B*, a serial desensitization model yields monotonically increasing steady state responses. The green line represents a simulation in which we chose parameters that yielded the best overlap to the rising phase of the concentration–response data. The purple line illustrates how reducing the glutamate K_d changes the outcome, which is still monotonic. The dashed line in *B* and *D* references the GluK2/GluK4 steady state concentration–response data found in Fig. 1*C*. The parallel desensitization model yielded similar results albeit with different parameters. Parameters for fits and simulations for all simulations and fits are given in Supplemental Material. *C*, schematic of model in which both GluK2 and the GluK4 or GluK5 subunits can bind glutamate. For clarity, K4 desensitized states are depicted in purple, while K2 desensitized states are shown in red. Binding of glutamate to at least two subunits allowed transition to an open state. Bold line transitions represent affinities for glutamate that have been allosterically modulated in a more

Table 1. Agonist concentration–response fits to specific activation and desensitization models

Model	Agonist	K_d GluK2	K_{desens} GluK2	K_d GluK4/5	K_{desens} GluK4/5	χ^2
Fits for GluK2/GluK4 agonist concentration response (Fig. 4)						
Serial desensitization	glu	< **1 nM***	0.3	—	0.1	1430
Parallel desensitization	glu	100 nM	0.005	—	**0.03**	1490
Binds GluK2 and GluK4	glu	**90.6 μM**	0.005	**407 nM**	10	4.7
Sequential fits for GluK2 and GluK2/GluK4 agonist concentration–response (Fig. 5)						
GluK2	glu	**106.8 μM**	0.005	—	—	4.0
GluK2/GluK4	glu	106.8 μM	0.005	**360 nM**	10	4.8
GluK2/GluK4	glu	200 μM	0.005	**213 nM**	10	7.7
Fits for agonist concentration response (Fig. 6)						
GluK2(E738D)/GluK4	glu	**25.1 mM**	0.005	213 nM	10	57.2
GluK2(E738D)/GluK4†	glu	**7.3 mM**	0.005	**708 nM**	10	1.5
GluK2/GluK4	AMPA	**17.5 mM**	0.005	**1.3 μM**	10	123
GluK2/GluK4	AMPA	**2.5 mM**	**0.12**	**1.6 μM**	10	119
GluK2/GluK5	AMPA	2.5 mM	0.12	**20.2 μM**	10	0.6
GluK2(E738D)/GluK4	AMPA	**24.5 mM**	0.12	1.6 μM	10	0.4

Emboldened values were results of data fits. Non-emboldened values were constants during fitting. K_d and K_{desens} values were calculated from the forward and reverse rate constants of the transition $k_{forward}/k_{reverse}$. Glu, glutamate; GluK4/5, GluK4 or GluK5 subunit. *Limited by constraints of fit. †Fit not shown on graph, but can be found in Supplemental Material.

the higher glutamate affinity and the non-desensitizing subunit (GluK4) forced to have the lower glutamate affinity, the resulting simulation was not biphasic (red line in Fig. 4*D*).

It is beyond the scope of this paper to rigorously define the kinetic rate constants for all transitions of the model depicted in Fig. 4*C*; however, our iterative procedure of fitting steady state concentration–response data (Fig. 4*D*) and then adjusting desensitization parameters to match onset and recovery data (Fig. 3) has led to parameters which approximate the data shown for GluK2/GluK4-expressing oocytes in Fig. 1*B*. Notable characteristics include steady state currents that increase with increasing glutamate concentrations to 0.3 μM but decrease thereafter, and tail currents observed upon removal of glutamate at concentrations > 0.3 μM (arrow in Fig. 4*E*). These simulated tail currents result from the dissociation of glutamate from its low-affinity binding site on the desensitizing subunit, which allows the channel to recover from desensitization prior to glutamate dissociation from its high-affinity binding site on the non-desensitizing subunit. Figure 5*A* graphically illustrates agonist action on each subunit suggested by the model in Fig. 4*C*, namely that low concentrations of agonist bind to high-affinity sites and open the heteromeric channel, whereas when low-affinity sites are occupied by higher concentrations of agonist, desensitization ensues.

Glutamate affinity and desensitization parameters determined for GluK2 homomers remain unchanged in the GluK2/GluK4 heteromeric model

If low- and high-affinity agonist binding sites reflect binding of glutamate to GluK2 and GluK4 subunits,

complex allosteric model (detailed in Supplemental Material). *D*, glutamate steady state concentration–response data were simulated utilizing the model presented in *C*. Simulations in which K_d and K_{desens} were set to the same values for both GluK2 and GluK4 subunits (purple line) yielded responses that increase with increasing glutamate concentration, as did simulations in which the K_d values at GluK2 and GluK4 differed by 30-fold but K_{desens} remained strongly desensitizing (green line). When K_{desens} was set to strongly desensitizing (0.005) and non-desensitizing (10) values for GluK2 and GluK4 subunits, respectively, and their respective glutamate K_d values fitted to glutamate steady state data for GluK2/GluK4, biphasic fits were obtained (blue line). The resulting K_d values indicate that the lower affinity K_d paired with the strongly desensitizing K_{desens} of 0.005, and the high-affinity K_d for glutamate paired with the non-desensitizing K_{desens} of 10 (Table 1). Conversely, when a simulation in which the strongly desensitizing K_{desens} of 0.005 was paired with the higher glutamate affinity K_d of 0.4 μM, and the non-desensitizing K_{desens} of 10 was paired with the lower glutamate affinity K_d of 91 μM, the results were *not* biphasic (red line). *E*, simulations of currents produced from the simultaneous fitting of the high- and low-affinity glutamate binding site parameters in *D* (blue line). Similar results were obtained for Fig. 5*B*. The filled circle indicates where simulated current amplitudes were measured during fitting. The arrow indicates the simulated tail current observed upon removal of 10 μM glutamate. The solution exchange time constant for this simulation was 3 s.

respectively, and the subunits function as somewhat independent modules, then we might expect that the binding and desensitization equilibrium constants attributed to the GluK2 subunit would be similar for fits of the model (Fig. 4*C*) to either GluK2 homomeric or GluK2/GluK4 heteromeric responses. The model shown in Fig. 4*C* can be adapted to GluK2 homomeric receptors by replacing the K4 subunit transitions (depicted in purple) with GluK2 subunit transitions (depicted in red). Such a model only has one K_d for glutamate and one K_{desens} value. When onset and recovery of desensitization were set to the values used for the strongly desensitizing subunit for successful fitting of the GluK2/GluK4 data (Fig. 4*D*, $K_{desens} = 0.005$), a fit of the homomeric GluK2 steady state concentration–response data yielded a K_d for glutamate binding of 107 μM (Fig. 5*B*, red line, and Table 1). Lower χ^2 values could be obtained by letting both K_d and K_{desens} vary during the fit, yet simulations of homomeric GluK2 utilizing these fitted parameters resulted in currents where the onset of desensitization was too slow or the recovery from desensitization was too rapid (data not shown). Using the 107 μM K_d value as a constant in a subsequent fit of the biphasic heteromeric GluK2/GluK4 data, the glutamate high-affinity binding constant could be determined with only one free parameter if the K_{desens} associated with high-affinity glutamate binding was non-desensitizing (K_{desens} for GluK4 = 10). The resulting fit had good overlap with the steady state concentration–response data and yielded a high-affinity glutamate K_d of 0.4 μM and a low χ^2 value for this data set (Supplemental Fig. 3 and Table 1). The kinetics for recovery from desensitization were similar to those in Fig. 3*D*, but the onset of desensitization decayed too rapidly. Adjusting GluK4 affinity had almost

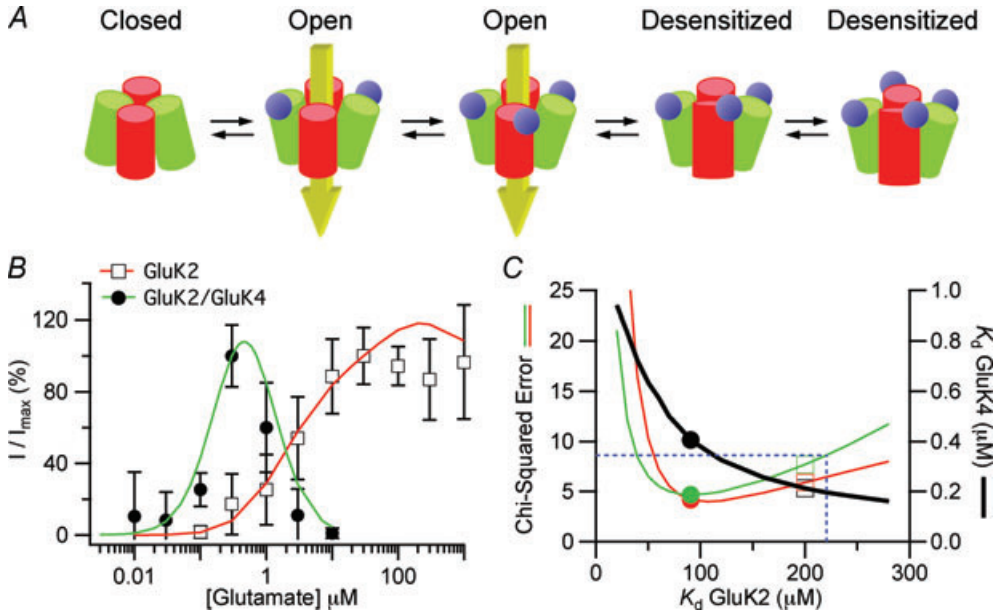

Figure 5. Parameters obtained from fitting the glutamate concentration–response of GluK2 homomeric receptors can be used to fit GluK2/GluK4 biphasic concentration–response data
A, illustration demonstrating agonist (blue ball) action at high-affinity (green) and low-affinity (red) subunit binding sites. Low concentrations of agonist preferentially bind to high-affinity sites and can open the channel and allow current flow (large arrow). Increasing the concentration of agonist will start to occupy low-affinity binding sites, desensitize the whole channel and prevent current flow. *B*, glutamate concentration–response curves obtained by analysing currents from oocytes expressing homomeric GluK2 (open squares) or GluK2/GluK4 (filled circles). Continuous lines indicate fits to the model depicted in Fig. 4*C*. In the case of homomeric GluK2 (red line), K2 subunits replace K4 subunits in the scheme, and there is only one K_d value and one K_{desens} value. K_{desens} was set to 0.005 and the K_d value determined from the fit (Table 1). The K_d parameter from the homomeric GluK2 data fit was then used as a constant in the fit of GluK2/GluK4 data where K_{desens} for GluK2 remained at 0.005, K_{desens} for GluK4 was set to 10 and the K_d value for GluK4 determined during fitting. The data were well fitted by this procedure (continuous green line). *C*, error analysis depicting how the χ^2 error of fits of GluK2 homomeric data (red line) and GluK2/GluK4 heteromeric data (green line) change with changing K_d values for GluK2 and GluK4. Bold black line indicates how the GluK4 K_d changes with the changing GluK2 K_d that was held constant during sequential fits. Open squares indicate the values obtained from the sequential fit for GluK2/GluK4 (*B*, green line). Filled circles indicate values obtained for the two parameter fit of the glutamate K_d values for GluK2 and GluK4 from the GluK2/GluK4 data (Fig. 4*D*, blue line and Table 1). Blue dashed lines indicate the upper bounds of the 95% confidence interval for the certainty of the glutamate K_d for GluK2 from fits of GluK2 homomeric data and the χ^2 error using this value in a fit of GluK2/GluK4 data.

no effect on the desensitization kinetics, whereas adjusting GluK2 glutamate binding affinity could profoundly affect these kinetics. By adjusting the K_d for glutamate at the GluK2 subunit to 200 μM, three criteria were fulfilled: (1) a good fit to GluK2 homomeric steady state data could still be obtained (red line, Fig. 5*B*); (2) the subsequent fit of the GluK4 K_d for glutamate of GluK2/GluK4 data keeping the GluK2 K_d for glutamate constant was also good (green line, Fig. 5*B*); and (3) the single exponential analysis for onset of desensitization ($\tau = 4.2$ and 99.1 ms for 1 mM and 10 μM glutamate, respectively) and recovery from desensitization ($\tau = 2.25$ s) were similar to experimental data (Fig. 3*B* and *D*). This sequential analysis of steady state concentration–response curves for GluK2- and GluK2/GluK4-expressing cells suggests that the GluK2 subunit moieties involved in glutamate binding and desensitization might not be strongly influenced by interactions with GluK4 subunits when incorporated into heteromers.

We know that these fitted parameters have a degree of uncertainty. Although the fits in Fig. 5*B* look good when assessed by eye, we wished to determine what variation in the glutamate K_d at the GluK2 subunit might be allowed. From the fit of homomeric GluK2 steady state data, 95% confidence intervals could be calculated for the K_d of glutamate binding to GluK2. This yielded an upper bound to the confidence interval of 221 μM (Blue dashed line, Fig. 5*C*) which has a much lower χ^2 value than the lower bound. We then systematically fitted GluK2/GluK4 data with different constant values for the glutamate K_d of GluK2 to determine fitted values for the glutamate K_d at GluK4 (bold line, Fig. 5*C*) and the corresponding χ^2 values (green line, Fig. 5*C*). In addition, χ^2 values for homomeric GluK2 simulations were also assessed (red line, Fig. 5*C*). The χ^2 value determined in the two parameter fit of the GluK2/GluK4 data predictably falls at the minimum of the χ^2 error curve and is also very close to the minimum of the GluK2 homomeric subunit error curve. The glutamate K_d value used in the final sequential fit of GluK2/GluK4 data (green line, Fig. 5*B*) falls within the confidence interval and the χ^2 error is lower than that utilizing the 221 μM value. This indicates that a K_d value of 200 μM for the GluK2 subunit is probably allowable.

Identification of the desensitizing subunit by an affinity-changing mutation in GluK2

Results from Figs 4 and 5 strongly suggest that the low affinity of glutamate and strong desensitization characteristics observed for homomeric GluK2 receptors are retained in heteromeric GluK2/GluK4 receptors. The data are also compatible with the notion that binding of glutamate to GluK4 is sufficient to open the channel without substantial desensitization. However, it is possible that in GluK2/GluK4 heteromeric channels significant changes in glutamate affinity and desensitization occur through the interaction of GluK2 with GluK4. We took advantage of the discovery of a GluK2 mutant with a very low affinity for glutamate to identify the desensitizing subunit of heteromeric kainate receptors.

Residue 738 was identified as a key conserved residue in the agonist S1S2 binding pocket of GluK2 (Mayer, 2005). A mutation from glutamate to aspartate at residue 738 caused a 260-fold decrease in the apparent affinity for glutamate measured from peak current amplitudes when compared to wildtype GluK2 receptors expressed in HEK-293 cells (Mah *et al.* 2005). In addition, macroscopic desensitization characteristics of this mutant appeared only slightly changed.

We confirmed that GluK2(E738D) exhibits reduced agonist affinity by measuring steady state concentration–response curves for glutamate-activating homomeric GluK2(E738D) receptors expressed in oocytes. Concentration–response analysis of the mutant homomer yielded an $n_e = 1.4$ and an $A_{1/2}$ value of 16.2 mM ($n = 6$ oocytes), which is a 9000-fold reduction in potency compared to wildtype GluK2 receptors (Fig. 6*B*, open triangles). This shift is much larger than the shift in apparent affinity of peak currents in HEK-293 cells (Mah *et al.* 2005). For heteromeric receptors, steady state glutamate concentration–response curves analysed from currents of both mutant GluK2(E738D)/GluK4 and wildtype GluK2/GluK4 had almost identical relative amplitudes for glutamate concentrations less than 1 μM (Fig. 6*B*). However, heteromers containing the mutant GluK2 subunit had significantly larger steady state currents (Fig. 6*A*) that peaked at 10–30 μM glutamate (Fig. 6*B*, filled triangles), compared to the peak at 0.3 μM of wildtype receptors (Fig. 1*C*, filled circles; Fig. 6*B*, crosses). Macroscopic desensitization for GluK2(E738D)/GluK4 channels was readily observed at glutamate concentrations greater than 30 μM (Fig. 6*A*) with almost complete desensitization occurring at 300 μM (Fig. 6*B*). Indeed, the declining phase of the glutamate concentration–response curve for GluK2(E738D)/GluK4 channels was right-shifted to a range of 30–300 μM (Fig. 6*B*) in comparison to wildtype GluK2/GluK4 controls (Fig. 1*C*). Upon removal of 300 μM glutamate, larger tail currents were observed for GluK2(E738D)/GluK4 channels in comparison to controls (Fig. 6*A*). This would be expected if dissociation of glutamate from its low-affinity binding site was rate limiting for the rising phase of the tail current.

A similar finding was also observed for AMPA concentration–response curves (Fig. 6*C*). The rising phases of AMPA concentration–response curves for wildtype GluK2/GluK4 and mutant GluK2(E738D)–GluK4 overlapped. In contrast, the declining phase of the AMPA concentration–response curves for the mutant

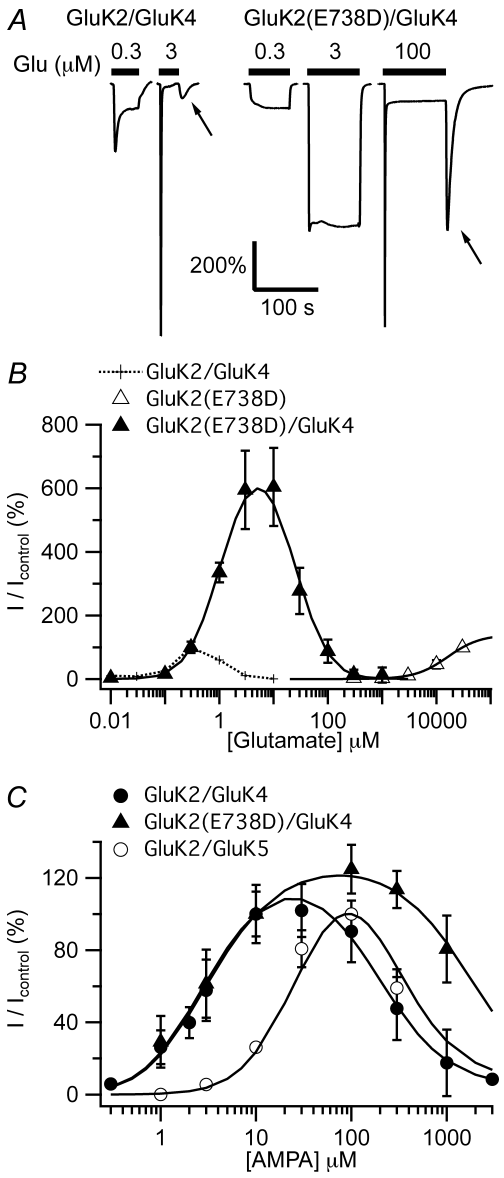

Figure 6. GluK2 subunits are responsible for the declining phase of steady state concentration–response curves
A, comparison of raw data responses to glutamate of wildtype GluK2/GluK4 and GluK2(E738D)/GluK4. Responses of each channel type have been normalized to the steady state current elicited by 0.3 μM glutamate (vertical scale bar is twice this amplitude). Note that wildtype responses show a strongly desensitizing current upon application of 3 μM glutamate and tail current upon exogenous glutamate removal (arrow). In contrast, GluK2(E738D)/GluK4 responses are larger and less desensitizing. Desensitization can be observed for GluK2(E738D)/GluK4 at higher concentrations of glutamate. Here too, removal of glutamate produces a swiftly rising tail current (arrow). *B*, glutamate concentration–response curves show that steady state responses to homomeric GluK2(E738D) (open triangles) have a 9000-fold higher $A_{1/2}$ value in comparison to GluK2 wildtype controls (not shown). Continuous line through the GluK2(E738D) homomeric data is the result of a fit utilizing eqn (2). GluK2(E738D)/GluK4 concentration–response data (filled triangles) yield higher steady state responses in comparison to wildtype GluK2/GluK4 (dotted line with crosses). Note that wildtype and mutant heteromeric receptors overlap in the rising phases of steady state glutamate concentration–response curves, but mutant decaying phase was right-shifted toward lower affinity. The current response used for normalizing responses ($I_{control}$) for both GluK2/GluK4 and GluK2(E738D)/GluK4 was measured at 0.3 μM glutamate, and 30 mM for glutamate for GluK2(E738D) homomeric receptors. The continuous line through the GluK2(E738D)/GluK4 data indicates the result from a fit to the experimental data of K_d values for glutamate binding for the GluK4 and mutant GluK2 subunits using the model depicted in Fig. 4*C*. *C*, the model presented in Fig. 4*C* was also fitted to AMPA concentration–response curves for GluK2/GluK4-expressing oocytes (filled circles) by fitting both high- and low-affinity AMPA K_d values simultaneously. AMPA concentration–response curves for responses from GluK2(E738D)/GluK4-expressing oocytes (filled triangles) showed the same rising phase as wildtype controls, but the decaying phase was right-shifted toward lower affinity. Fits of the model to GluK2(E738D)/GluK4 data were done by using the GluK4 AMPA K_d value determined from the wildtype GluK2/GluK4 fit as a constant in the fit of the AMPA K_d for GluK2(E738D). Experimental data acquired for GluK2/GluK5 are also shown for comparison (open circles). Here the rising phase of the concentration–response curve is right-shifted with respect to that of the GluK2/GluK4 data, but the decaying phases of both curves overlap. For fitting the model to GluK2/GluK5 data, the glutamate K_d value for GluK2 determined in the fit of GluK2/GluK4 data was used as a constant in the fit of the glutamate K_d value for GluK5. AMPA concentrations for measuring $I_{control}$ values were 10 μM for GluK2/GluK4 and GluK2(E738D)/GluK4 AMPA concentration–response curves, and 100 μM for GluK2/GluK5 AMPA concentration–response curve. Fits to the model are depicted as continuous lines. Fitted and constant parameters are summarized in Table 1.

(filled triangles) was right-shifted in comparison to wildtype. Since the mutation resides on the GluK2 subunit, these data strongly suggest that the decaying phase of the AMPA and glutamate concentration–response curves results from the action of agonist binding to the GluK2 subunit, which as in homomeric GluK2 receptors, causes strong desensitization. In addition, overlap of the rising phases of the concentration–response curves for heteromeric wildtype and mutant channels suggests that GluK4, the invariant subunit in these heteromeric channel combinations, binds AMPA with high affinity and produces little or no desensitization. For comparison, an AMPA concentration–response curve is also shown for the GluK2/GluK5 subunit combination (Fig. 6*C*). Here, the rising phase of the concentration–response curve is right-shifted in comparison to the GluK2/GluK4 wildtype and mutant curves, but the decaying phase falls on that of the GluK2/GluK4 wildtype curve. This also suggests that the common subunit, GluK2, is responsible for the decaying phase of the concentration–response curve, whereas the differing subunits, GluK4 or GluK5, are responsible for the rising phase.

We fitted the mutant data to our model depicted in Fig. 4*C* in order to determine if the GluK4 subunit was still acting somewhat independently of the mutant GluK2 subunit with respect to its binding and desensitization properties. Since wildtype GluK4 subunits are common to

both GluK2/GluK4 and GluK2(E738D)/GluK4 receptors, we held constant the glutamate K_d for GluK4 (213 nM) determined in Fig. 5*B* and fitted the glutamate K_d for the mutant GluK2 subunits to the GluK2(E738D)/GluK4 biphasic data. This sequential fit showed a biphasic trend that approximated the data except at the highest responses produced by 1, 3 and 10 μM glutamate (Supplemental Fig. 4 and Table 1). When the glutamate K_d values for both the GluK4 and GluK2(E738D) subunits were simultaneously fitted, a good fit was obtained. As expected, the K_d for the mutant GluK2 subunit was 81-fold higher than the K_d value found from the two-parameter fit of wildtype GluK2/GluK4 data (Table 1, Fig. 6*B*). However, the GluK4 K_d value of 708 nM was also 1.7-fold higher than that found for the wildtype channel.

To evaluate if the glutamate K_d value for GluK4 from the fit of the GluK2(E738D)/GluK4 data significantly differs from that derived from the wildtype GluK2/GluK4 data, we analysed the uncertainty of this value. The 708 nM K_d for glutamate binding to the GluK4 subunit in the mutant heteromer is within the 95% confidence interval for the glutamate K_d determined for the wildtype heteromeric data (upper limit of 731 nM). This may indicate that the affinity of glutamate for the GluK4 subunit does not significantly change when GluK4 is complexed with wildtype GluK2 or the mutant GluK2 subunits.

The biphasic AMPA dose–response curves were also fitted to the model in Fig. 4*C*. A summary of different fitting trials indicates that the data could be fitted with a variety of values for K_{desens} for GluK2. The AMPA concentration–response curve for the GluK2/GluK4 subunit combination was fitted for two AMPA K_d values and utilizing the K_{desens} values of 0.005 and 10 used previously for the glutamate data as constants (Fig. 5*B*). This yielded an affinity for AMPA of 1.3 μM and 17.5 mM at the GluK4 and GluK2 subunits, respectively (Fig. 6*C*, Table 1, $n = 26$ oocytes). However, K_{desens} values may be different than those of glutamate. When doing a three-parameter fit of the two K_d values for AMPA and one K_{desens} value (keeping the second K_{desens} value constant at 10), a 24-fold larger K_{desens} value was obtained (Table 1), but the K_d values still associated in the same manner: the high-affinity K_d was linked to the non-desensitizing K_{desens}, and the low-affinity K_d was linked with strong desensitization (Table 1). These examples illustrate that there is a strong correlation between the degree of desensitization of GluK2 and AMPA binding affinity at that site. However, with either fit, binding of AMPA to the GluK2 subunit is at least 28-fold weaker than glutamate binding to the same subunit, whereas AMPA binding to the non-desensitizing GluK4 subunit is only 4-fold weaker (Table 1). The disproportionate changes in affinity for agonist binding at the different subunits reflect the fact that the AMPA concentration–response curve is broader than the glutamate curve (Fig. 1*C* and *D*).

Since the GluK2(E738D)/GluK4 and wildtype GluK2/GluK4 share the GluK4 subunit, we can use the AMPA K_d value determined for the GluK4 subunit from the wildtype GluK2/GluK4 fit for a sequential fit of the K_d value of the GluK2(E738D) subunit from the mutant concentration–response curve. Figure 6*C* shows that GluK2(E738D)/GluK4 steady state responses were fitted well in this manner, and yielded a K_d of 24.5 mM for the GluK2(E738D) subunit ($n = 5$ oocytes), 9.8-fold lower affinity than K_d for AMPA determined for wildtype GluK2 in the fit of GluK2/GluK4 under similar conditions (Table 1).

Finally, one can also fit the AMPA concentration–response curve for GluK2/GluK5 to the model in Fig. 4*C*. Since the wildtype GluK2 subunit is common to both GluK2/GluK4 and GluK2/GluK5 channels, it may be possible to utilize the GluK2 K_d found in the fit of the AMPA concentration–response from GluK2/GluK4 as a constant in the fit to determine the AMPA K_d for GluK5 from GluK2/GluK5 steady state responses. These data were well fitted by this sequential strategy, and yielded a K_d for the putative GluK5 subunit of 20.2 μM, 12.6-fold lower affinity than what was found for the GluK4 subunit in wildtype heteromeric receptors (Table 1). The fact that GluK2(E738D)/GluK4 responses can be successfully fitted without changing the GluK4 K_d for agonist determined from the fit of wildtype GluK2/GluK4 responses, and that GluK2/GluK5 responses can be successfully fitted without changing the GluK2 K_d for agonist determined from GluK2/GluK4 responses, suggests that GluK2 and GluK4 subunits do not have large interaction with respect to agonist binding.

Discussion

Mechanistic autonomy of subunit action for heteromeric kainate receptors

This study has shown that heteromeric kainate receptors containing GluK2 and either GluK4 or GluK5 subunits possess binding and desensitization characteristics that can be localized to the particular subunit subtypes. We have exploited the *Xenopus* oocyte expression system which allows us to express heteromeric kainate receptors at high expression levels so as to observe their biphasic, bell-shaped steady state concentration–response curves. The oocyte expression system cannot resolve temporal resolution of channel activity on the millisecond time scale required to resolve macroscopic desensitization of kainate receptors. However, the concentration dependence of the onset of desensitization (Fig. 3*A*–*C*) or the kinetics of recovery from desensitization (Fig. 3*D* and *E*) obtained from the HEK-293 cell expression system, where temporal resolution is adequate, can be produced by multiple mechanisms of action. In fact, we argue

that the additional observation of the biphasic steady state concentration–response curves enabled by the oocyte expression system is critical to deduce that agonist binding and desensitization properties are strikingly different between the GluK2 and GluK4 or GluK5 subunits.

Using the general model presented in Fig. 4*C*, we have shown that two types of binding sites for agonists exist: a high-affinity, non-desensitizing site and a low-affinity strongly desensitizing site. A right-ward shift in the decaying phase of the biphasic steady state concentration–response curve was observed when the low apparent binding affinity mutant, GluK2(E738D), was substituted for wildtype GluK2 subunits in heteromeric combination with GluK4 subunits (Fig. 6). The rising phase of the agonist concentration–response curves overlapped for both mutant GluK2(E738D)/GluK4- and wildtype GluK2/GluK4-containing receptors. This suggests that the two types of binding and desensitization properties described by the model can be isolated to either the GluK2 or GluK4 subunit. Furthermore, simulations with our model suggest that affinity and desensitization properties of agonists are similar for GluK2 subunits as either homomers or when incorporated into heteromeric combination with GluK4 subunits (Figs 5*B*, 6*B* and *C*). The fact that the GluK4 and GluK5 subunit is responsible for the higher affinity rising phase of concentration–response curves for GluK2/GluK4 and GluK2/GluK5 (Figs 1C, *D*, 6*B* and *C*) corroborates radioligand binding data for glutamate indicating that the GluK5 subunit has a higher K_i in comparison to the GluK2 subunit (Egebjerg *et al.* 1991; Herb *et al.* 1992). One can also note that recovery from glutamate-induced desensitization is similar for GluK2 (Heckmann *et al.* 1996) and GluK2/GluK4 (Fig. 3*D*) as well as for GluK2/GluK5 (Barberis *et al.* 2008). Together this evidence suggests that GluK2 subunits behave rather autonomously with respect to agonist binding and are responsible for desensitization and recovery of heteromeric kainate receptors.

However, one could argue that some interaction between GluK2 and GluK4 subunits must occur to change the specificity of AMPA for the GluK2 binding site, since AMPA can act as an agonist for GluK2/GluK4 subunits within a heteromer (Fig. 1*D*), but has been reported not to elicit currents from GluK2 homomeric channels (Egebjerg *et al.* 1991; Swanson *et al.* 1997). Table 1 indicates that fits of the model to the biphasic AMPA concentration–response curve for GluK2/GluK4 yielded an apparent K_d value for GluK2 of 2.5 mM when K_{desens} was 0.12. K_d values were even higher for lower K_{desens} values (Table 1). Simulations of GluK2 homomeric receptor activity utilizing AMPA as an agonist with this K_d indicate that steady state currents would not be resolved at AMPA concentrations below 1 mM (data not shown). In line with this analysis, we were able to observe very small currents from oocytes expressing GluK2 homomeric channels in response to application of 1 mM AMPA (Supplemental Fig. 5). Although resolvable currents are small, our analysis indicates that a significant number of GluK2 receptors would be bound with AMPA, even at lower concentrations, but those receptors have a high probability of residing in high-affinity desensitized states. According to our simulations of homomeric GluK2 binding, 9% of AMPA binding sites would be occupied at 30 μM AMPA and 35% of the binding sites would be occupied at 300 μM AMPA (data not shown). Together this indicates that a change in AMPA binding site specificity for GluK2 subunits is *not* required to explain the discrepancy between the concentration of AMPA required to cause the onset of the declining phase for GluK2/GluK4 and GluK2/GluK5 concentration–response curves (Fig. 6*C*) and the first observation of steady state current at ~1 mM AMPA.

This heteromeric model could be generalized to other kainate receptor subunit combinations involving GluK4 and GluK5. Long-lasting tail currents were elicited from HEK-293 cells expressing either GluK1/GluK5 or GluK2/GluK5 subunits upon removal of dysiherbaine, a high-affinity, highly desensitizing, kainate receptor agonist. However, tail currents were not observed in responses from GluK1/GluK4-containing subunits or homomeric GluK1 or GluK2 channels (Swanson *et al.* 2002). For tail currents to be observed, partial recovery from desensitization must occur prior to agonist dissociation. Binding studies suggest that dysiherbaine has a lower affinity for GluK4 and GluK5 subunits than for GluK1. The kinetics and degree of desensitization induced at kainate receptors differ for different agonists, and allosteric interactions between binding sites on different subunits may also be agonist specific. It may be possible to address these issues and test if the heteromeric model (Fig. 4*C*) can be generalized to GluK1- and GluK3-containing heteromers with further experiments utilizing low apparent affinity mutants as was done for GluK2 in Fig. 6. Recently, Barberis *et al.* (2008) reported that expression of GluK5 with GluK2 has a 13.5-fold slower deactivation to a 1.5 ms pulse of glutamate than GluK2 homomeric receptors. Their simulations concur with our findings that GluK4 or GluK5 subunits have a higher affinity for glutamate and desensitize less than the GluK2 subunit.

Biphasic steady state concentration–response curves have also been observed in response to exogenous applications of kainate and glutamate on cultured neurons containing 'native' kainate receptors. Yet, biphasic steady state concentration–response curves were not observed for GluK2 recombinant receptor responses in the same study (Paternain *et al.* 1998). These results are consistent with a high proportion of native kainate receptors in these cultured neurons containing both GluK1/3 and GluK4/5

subunits. However, it should be noted that the steady state responses elicited from cultured neurons peaked at 30 μM glutamate, approximately 100-fold higher than the peak of the GluK2/GluK4 steady state dose–response curve (Fig. 1*C*). This could result if cultured neurons had a different combination of GluK1/3 and GluK4/5 subunits than GluK2/GluK4 or from modulation of heteromeric receptor function by natively expressed auxiliary proteins (Hirbec *et al.* 2003; Laezza *et al.* 2008; Zhang *et al.* 2009).

Role of heteromeric kainate receptors in synaptic transmission

Kainate receptors modulate presynaptic neurotransmitter release and can mediate postsynaptic currents (Pinheiro & Mulle, 2006 for review). Expression of individual kainate receptor subunits varies widely in the adult (Wisden & Seeburg, 1993) and developing brains (Bahn *et al.* 1994) with a high incidence of co-localization of GluK1/3 with GluK5 in many regions. GluK4 is mainly expressed in the CA3 region of the hippocampus. The threshold concentration of glutamate required to activate heteromeric kainate receptors at equilibrium is approximately 100 nM (Fig. 1*C*), above the ambient glutamate concentration in hippocampus of 25 nM estimated by Herman & Jahr (2007). The low ambient glutamate concentration assures that kainate receptors will normally only be activated upon synaptic release of glutamate. However, under pathological conditions such as stroke, ambient glutamate concentrations may be orders of magnitude higher (Benveniste *et al.* 1984; Davalos *et al.* 1997). In this case, tonic excitation of heteromeric kainate receptors might be shut down by desensitization of the channel by GluK2.

Our results predict that presynaptic modulation of synaptic transmission by direct ionotropic action of heteromeric kainate receptors would occur only within a narrow band of agonist concentration. A salient example is the action of domoate on parallel fibre presynaptic terminals in the cerebellum (Delaney & Jahr, 2002). Parallel fibre–stellate cell EPSCs were potentiated during the application of 5 nM domoate, but inhibited by higher domoate concentrations. This occurred despite the lack of change in the parallel fibre–afferent fibre volley. In contrast, parallel fibre–Purkinje cell EPSCs were potentiated rather than inhibited by 50 nM domoate. As Delaney and Jahr noted, those results would suggest that two different kainate receptor subunit combinations exist at these two parallel fibre synapses. In light of the results presented here, we would suggest that parallel fibre–stellate cell synapses contain a combination of GluK1/3 and GluK4/5 subunits, while parallel fibre–Purkinje cell synapses have kainate receptor channels composed of only GluK1/3 subunits. GluK2 and GluK5 subunits have been localized to parallel fibres by immunohistochemistry (Petralia *et al.* 1994).

Utilizing our model of heteromeric kainate receptor function, we can approximate characteristics that we might observe from synaptic currents mediated by GluK2/GluK4 heteromers by simulating the response to a 1 ms pulse of glutamate (Fig. 7). From a 1 mM pulse, we would expect a rapidly decaying component followed by a long-lasting tail. The kinetics of the long-lasting tail are dependent on the affinity of glutamate for the GluK4 subunit. In the absence of the GluK4 subunit, homomeric GluK2 receptor-mediated currents would be expected to completely decay within 5 ms (Fig. 7*A*). A rapidly decaying component of the EPSC has not been observed for responses putatively mediated by GluK2/GluK4 receptors (Fernandes *et al.* 2009). Interestingly, the rapid component of the simulated biphasic decay of GluK2/GluK4 receptors is highly sensitive to the concentration of glutamate pulsed. At glutamate concentrations of 100 μM and below, only the slowly decaying component can be observed (Fig. 7*B*). Immunogold labelling of heteromeric kainate receptors

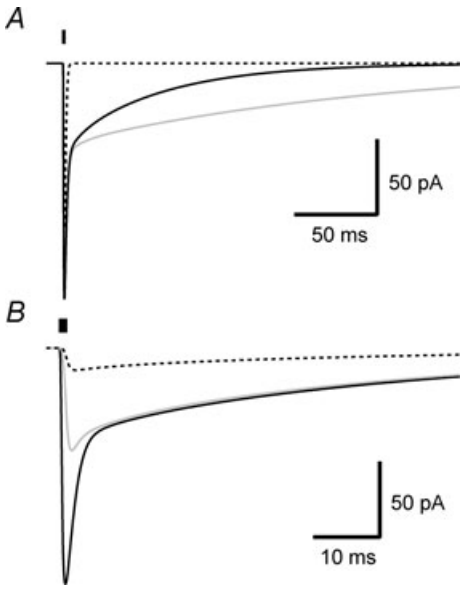

Figure 7. Simulation of heteromeric kainate receptor synaptic responses
Synaptic currents mediated by GluK2/GluK4 receptors were created by simulating the response under voltage clamp to a 1 ms pulse of glutamate (black bar). The solution exchange time constant was 0.5 ms. *A*, model depicted in Fig. 4*C* was used in a simulation of the response to 1 mM glutamate with parameters for homomeric GluK2 receptors (dashed line), heteromeric GluK2/GluK4 parameters in which the K_d for the GluK4 subunit was set either to 213 nM (grey continuous line) or 708 nM (black continuous line). The decay of the slow component was strongly dependent on the K_d of GluK4. *B*, responses of GluK2/GluK4 heteromeric receptors to either 30 μM (dashed line), 100 μM (grey continuous line) or 1 mM glutamate (black continuous line). The parameters used were the same as for the black continuous line in *A*. The slowly decaying component is apparent at all concentrations of glutamate, whereas the rapidly decaying component is only observed above 100 μM glutamate.

showed significant labelling in perisynaptic as well as synaptic regions of postsynaptic neurons (Darstein *et al.* 2003; Fernandes *et al.* 2009). As synaptically released glutamate is expected to be of lower concentration at perisynaptic regions, it is possible that the combined response from synaptic and perisynaptic regions may hide the rapidly decaying component. Determination of kinetic constants and conductances of the multiple open states may also help elucidate this discrepancy.

Our results clearly demonstrate that GluK4 and GluK5 subunits have distinct ionotropic function within heteromeric receptors. Recently, it has been shown that GluK4 and GluK5 knockout mice had no kainate receptor-mediated EPSCs at mossy fibre–CA3 synapses. This correlates with changes in synaptic and perisynaptic distribution of GluK2 or GluK3 despite unchanged overall expression of these subunits in comparison to wildtype animals (Fernandes *et al.* 2009). This suggests that GluK4 or GluK5 subunits are required for functional expression of the postsynaptic kainate receptor at these synapses and that GluK2 and GluK3 play a modulatory role of limiting current duration through desensitization. If this is the case, a new focus on GluK4 and GluK5 subunits as therapeutic targets for pharmaceuticals may prove to be more effective in treatment of neurobiological disease such as epilepsy.

References

Alt A, Weiss B, Ogden AM, Knauss JL, Oler J, Ho K, Large TH & Bleakman D (2004). Pharmacological characterization of glutamatergic agonists and antagonists at recombinant human homomeric and heteromeric kainate receptors *in vitro*. *Neuropharmacology* **46**, 793–806.

Bahn S, Volk B & Wisden W (1994). Kainate receptor gene expression in the developing rat brain. *J Neurosci* **14**, 5525–5547.

Bannister NJ, Benke TA, Mellor J, Scott H, Gurdal E, Crabtree JW & Isaac JT (2005). Developmental changes in AMPA and kainate receptor-mediated quantal transmission at thalamocortical synapses in the barrel cortex. *J Neurosci* **25**, 5259–5271.

Barberis A, Sachidhanandam S & Mulle C (2008). GluR6/KA2 kainate receptors mediate slow-deactivating currents. *J Neurosci* **28**, 6402–6406.

Benveniste H, Drejer J, Schousboe A & Diemer NH (1984). Elevation of the extracellular concentrations of glutamate and aspartate in rat hippocampus during transient cerebral ischemia monitored by intracerebral microdialysis. *J Neurochem* **43**, 1369–1374.

Benveniste M, Clements J, Vyklicky Jr L & Mayer ML (1990). A kinetic analysis of the modulation of *N*-methyl-D-aspartic acid receptors by glycine in mouse cultured hippocampal neurones. *J Physiol* **428**, 333–357.

Castillo PE, Malenka RC & Nicoll RA (1997). Kainate receptors mediate a slow postsynaptic current in hippocampal CA3 neurons. *Nature* **388**, 182–186.

Chesnut JD, Baytan AR, Russell M, Chang MP, Bernard A, Maxwell IH & Hoeffler JP (1996). Selective isolation of transiently transfected cells from a mammalian cell population with vectors expressing a membrane anchored single-chain antibody. *J Immunol Methods* **193**, 17–27.

Contractor A, Sailer AW, Darstein M, Maron C, Xu J, Swanson GT & Heinemann SF (2003). Loss of kainate receptor-mediated heterosynaptic facilitation of mossy-fibre synapses in KA2$^{-/-}$ mice. *J Neurosci* **23**, 422–429.

Contractor A, Swanson GT, Sailer A, O'Gorman S & Heinemann SF (2000). Identification of the kainate receptor subunits underlying modulation of excitatory synaptic transmission in the CA3 region of the hippocampus. *J Neurosci* **20**, 8269–8278.

Cossart R, Epsztein J, Tyzio R, Becq H, Hirsch J, Ben-Ari Y & Crepel V (2002). Quantal release of glutamate generates pure kainate and mixed AMPA/kainate EPSCs in hippocampal neurons. *Neuron* **35**, 147–159.

Cossart R, Esclapez M, Hirsch JC, Bernard C & Ben-Ari Y (1998). GluR5 kainate receptor activation in interneurons increases tonic inhibition of pyramidal cells. *Nat Neurosci* **1**, 470–478.

Darstein M, Petralia RS, Swanson GT, Wenthold RJ & Heinemann SF (2003). Distribution of kainate receptor subunits at hippocampal mossy fibre synapses. *J Neurosci* **23**, 8013–8019.

Davalos A, Castillo J, Serena J & Noya M (1997). Duration of glutamate release after acute ischemic stroke. *Stroke* **28**, 708–710.

Delaney AJ & Jahr CE (2002). Kainate receptors differentially regulate release at two parallel fibre synapses. *Neuron* **36**, 475–482.

Dingledine R, Borges K, Bowie D & Traynelis SF (1999). The glutamate receptor ion channels. *Pharmacol Rev* **51**, 7–61.

Egebjerg J, Bettler B, Hermans-Borgmeyer I & Heinemann S (1991). Cloning of a cDNA for a glutamate receptor subunit activated by kainate but not AMPA. *Nature* **351**, 745–748.

Fernandes HB, Catches JS, Petralia RS, Copits BA, Xu J, Russell TA, Swanson GT & Contractor A (2009). High-affinity kainate receptor subunits are necessary for ionotropic but not metabotropic signalling. *Neuron* **63**, 818–829.

Frerking M, Malenka RC & Nicoll RA (1998). Synaptic activation of kainate receptors on hippocampal interneurons. *Nat Neurosci* **1**, 479–486.

Frerking M, Schmitz D, Zhou Q, Johansen J & Nicoll RA (2001). Kainate receptors depress excitatory synaptic transmission at CA3→CA1 synapses in the hippocampus via a direct presynaptic action. *J Neurosci* **21**, 2958–2966.

Heckmann M, Bufler J, Franke C & Dudel J (1996). Kinetics of homomeric GluR6 glutamate receptor channels. *Biophys J* **71**, 1743–1750.

Herb A, Burnashev N, Werner P, Sakmann B, Wisden W & Seeburg PH (1992). The KA-2 subunit of excitatory amino acid receptors shows widespread expression in brain and forms ion channels with distantly related subunits. *Neuron* **8**, 775–785.

Herman MA & Jahr CE (2007). Extracellular glutamate concentration in hippocampal slice. *J Neurosci* **27**, 9736–9741.

Hirbec H, Francis JC, Lauri SE, Braithwaite SP, Coussen F, Mulle C, Dev KK, Coutinho V, Meyer G, Isaac JT, Collingridge GL & Henley JM (2003). Rapid and differential regulation of AMPA and kainate receptors at hippocampal mossy fibre synapses by PICK1 and GRIP. *Neuron* **37**, 625–638.

Huettner JE (1990). Glutamate receptor channels in rat DRG neurons: activation by kainate and quisqualate and blockade of desensitization by Con A. *Neuron* **5**, 255–266.

Kidd FL, Coumis U, Collingridge GL, Crabtree JW & Isaac JT (2002). A presynaptic kainate receptor is involved in regulating the dynamic properties of thalamocortical synapses during development. *Neuron* **34**, 635–646.

Kohler M, Burnashev N, Sakmann B & Seeburg PH (1993). Determinants of Ca^{2+} permeability in both TM1 and TM2 of high affinity kainate receptor channels: diversity by RNA editing. *Neuron* **10**, 491–500.

Kwon HB & Castillo PE (2008). Role of glutamate autoreceptors at hippocampal mossy fibre synapses. *Neuron* **60**, 1082–1094.

Laezza F, Wilding TJ, Sequeira S, Craig AM & Huettner JE (2008). The BTB/kelch protein, KRIP6, modulates the interaction of PICK1 with GluR6 kainate receptors. *Neuropharmacology* **55**, 1131–1139.

Mah SJ, Cornell E, Mitchell NA & Fleck MW (2005). Glutamate receptor trafficking: endoplasmic reticulum quality control involves ligand binding and receptor function. *J Neurosci* **25**, 2215–2225.

Mayer ML (2005). Crystal structures of the GluR5 and GluR6 ligand binding cores: molecular mechanisms underlying kainate receptor selectivity. *Neuron* **45**, 539–552.

Mott DD, Benveniste M & Dingledine RJ (2008). pH-dependent inhibition of kainate receptors by zinc. *J Neurosci* **28**, 1659–1671.

Mott DD, Washburn MS, Zhang S & Dingledine RJ (2003). Subunit-dependent modulation of kainate receptors by extracellular protons and polyamines. *J Neurosci* **23**, 1179–1188.

Mulle C, Sailer A, Perez-Otano I, Dickinson-Anson H, Castillo PE, Bureau I, Maron C, Gage FH, Mann JR, Bettler B & Heinemann SF (1998). Altered synaptic physiology and reduced susceptibility to kainate-induced seizures in GluR6-deficient mice. *Nature* **392**, 601–605.

Mulle C, Sailer A, Swanson GT, Brana C, O'Gorman S, Bettler B & Heinemann SF (2000). Subunit composition of kainate receptors in hippocampal interneurons. *Neuron* **28**, 475–484.

Nahum-Levy R, Fossom LH, Skolnick P & Benveniste M (1999). Putative partial agonist 1-aminocyclopropanecarboxylic acid acts concurrently as a glycine-site agonist and a glutamate-site antagonist at N-methyl-D-aspartate receptors. *Mol Pharmacol* **56**, 1207–1218.

Nasu-Nishimura Y, Hurtado D, Braud S, Tang TT, Isaac JT & Roche KW (2006). Identification of an endoplasmic reticulum-retention motif in an intracellular loop of the kainate receptor subunit KA2. *J Neurosci* **26**, 7014–7021.

Paternain AV, Herrera MT, Nieto MA & Lerma J (2000). GluR5 and GluR6 kainate receptor subunits coexist in hippocampal neurons and coassemble to form functional receptors. *J Neurosci* **20**, 196–205.

Paternain AV, Rodriguez-Moreno A, Villarroel A & Lerma J (1998). Activation and desensitization properties of native and recombinant kainate receptors. *Neuropharmacology* **37**, 1249–1259.

Petralia RS, Wang YX & Wenthold RJ (1994). Histological and ultrastructural localization of the kainate receptor subunits, KA2 and GluR6/7, in the rat nervous system using selective antipeptide antibodies. *J Comp Neurol* **349**, 85–110.

Pinheiro P & Mulle C (2006). Kainate receptors. *Cell Tissue Res* **326**, 457–482.

Pinheiro PS, Perrais D, Coussen F, Barhanin J, Bettler B, Mann JR, Malva JO, Heinemann SF & Mulle C (2007). GluR7 is an essential subunit of presynaptic kainate autoreceptors at hippocampal mossy fibre synapses. *Proc Natl Acad Sci U S A* **104**, 12181–12186.

Ren Z, Riley NJ, Garcia EP, Sanders JM, Swanson GT & Marshall J (2003). Multiple trafficking signals regulate kainate receptor KA2 subunit surface expression. *J Neurosci* **23**, 6608–6616.

Robert A, Armstrong N, Gouaux JE & Howe JR (2005). AMPA receptor binding cleft mutations that alter affinity, efficacy, and recovery from desensitization. *J Neurosci* **25**, 3752–3762.

Robert A & Howe JR (2003). How AMPA receptor desensitization depends on receptor occupancy. *J Neurosci* **23**, 847–858.

Rodriguez-Moreno A, Lopez-Garcia JC & Lerma J (2000). Two populations of kainate receptors with separate signalling mechanisms in hippocampal interneurons. *Proc Natl Acad Sci U S A* **97**, 1293–1298.

Sanders JM, Ito K, Settimo L, Pentikainen OT, Shoji M, Sasaki M, Johnson MS, Sakai R & Swanson GT (2005). Divergent pharmacological activity of novel marine-derived excitatory amino acids on glutamate receptors. *J Pharmacol Exp Ther* **314**, 1068–1078.

Sanders JM, Pentikainen OT, Settimo L, Pentikainen U, Shoji M, Sasaki M, Sakai R, Johnson MS & Swanson GT (2006). Determination of binding site residues responsible for the subunit selectivity of novel marine-derived compounds on kainate receptors. *Mol Pharmacol* **69**, 1849–1860.

Schmitz D, Frerking M & Nicoll RA (2000). Synaptic activation of presynaptic kainate receptors on hippocampal mossy fibre synapses. *Neuron* **27**, 327–338.

Smolders I, Bortolotto ZA, Clarke VR, Warre R, Khan GM, O'Neill MJ, Ornstein PL, Bleakman D, Ogden A, Weiss B, Stables JP, Ho KH, Ebinger G, Collingridge GL, Lodge D & Michotte Y (2002). Antagonists of GLU(K5)-containing kainate receptors prevent pilocarpine-induced limbic seizures. *Nat Neurosci* **5**, 796–804.

Swanson GT, Feldmeyer D, Kaneda M & Cull-Candy SG (1996). Effect of RNA editing and subunit co-assembly single-channel properties of recombinant kainate receptors. *J Physiol* **492**, 129–142.

Swanson GT, Gereau RWt, Green T & Heinemann SF (1997). Identification of amino acid residues that control functional behaviour in GluR5 and GluR6 kainate receptors. *Neuron* **19**, 913–926.

Swanson GT, Green T & Heinemann SF (1998). Kainate receptors exhibit differential sensitivities to (S)-5-iodowillardiine. *Mol Pharmacol* **53**, 942–949.

Swanson GT, Green T, Sakai R, Contractor A, Che W, Kamiya H & Heinemann SF (2002). Differential activation of individual subunits in heteromeric kainate receptors. *Neuron* **34**, 589–598.

Werner P, Voigt M, Keinanen K, Wisden W & Seeburg PH (1991). Cloning of a putative high-affinity kainate receptor expressed predominantly in hippocampal CA3 cells. *Nature* **351**, 742–744.

Wilding TJ & Huettner JE (1996). Antagonist pharmacology of kainate- and alpha-amino-3-hydroxy-5-methyl-4-isoxazolepropionic acid-preferring receptors. *Mol Pharmacol* **49**, 540–546.

Wisden W & Seeburg PH (1993). A complex mosaic of high-affinity kainate receptors in rat brain. *J Neurosci* **13**, 3582–3598.

Wong LA & Mayer ML (1993). Differential modulation by cyclothiazide and concanavalin A of desensitization at native α-amino-3-hydroxy-5-methyl-4-isoxazolepropionic acid- and kainate-preferring glutamate receptors. *Mol Pharmacol* **44**, 504–510.

Zhang W, St-Gelais F, Grabner CP, Trinidad JC, Sumioka A, Morimoto-Tomita M, Kim KS, Straub C, Burlingame AL, Howe JR & Tomita S (2009). A transmembrane accessory subunit that modulates kainate-type glutamate receptors. *Neuron* **61**, 385–396.

Author contributions

D.D.M. and M.B. were primarily responsible for experimental design. D.D.M., R.J.D., A.R., J.L.F. and M.B. gave input on experimental design, were involved intellectually and were responsible for manuscript preparation. D.D.M., A.R., J.L.F. and M.B. were responsible for data collection. M.B. was responsible for data analysis and had overall responsibility for all aspects of the study.

Acknowledgements

This work was supported by grants from the National Institute of Neurological Disease and Stroke (1R01NS065869 to D.D.M. and J.L.F., S11NS055883 to M.B., 5R01 NS036604 to R.J.D.) and from the South Carolina Research Foundation (D.D.M.) and NARSAD (D.D.M.). The authors would also like to thank Renee Shaw and Antoine G. Almonte for their expert technical assistance in cRNA production and oocyte preparation.